ORGANOMETALLICS
Article
Cite This: Organometallics XXXX, XXX, XXX–XXX
pubs.acs.org/Organometallics

Bioactive Heterobimetallic Re(I)/Au(I) Complexes Containing Bidentate N-Heterocyclic Carbenes

Andrés Luengo,[†] Vanesa Fernández-Moreira,*[,†] Isabel Marzo,[‡] and M. Concepción Gimeno*[,†]

[†]Departamento de Química Inorgánica, Instituto de Síntesis Química y Catálisis Homogénea (ISQCH), CSIC-Universidad de Zaragoza, Pedro Cerbuna 12, 50009 Zaragoza, Spain

[‡]Departamento de Bioquímica y Biología Molecular, Universidad de Zaragoza, Pedro Cerbuna 12, 50009 Zaragoza, Spain

Supporting Information

ABSTRACT: The first cationic heterobimetallic complexes of the type *fac*-[Re(CO)$_3$(NHC)(LAuPPh$_3$)]$^+$, where NHC is an imidazole pyridine-based carbene and L is 3-pyridylalkyne, 4-pyridylalkyne, or 5-ethynyl-1-methyl-1*H*-imidazole, have been synthesized together with their Re(I) precursors. All of them have showed similar emissive properties resulting from the presence of the NHC system within the Re(I) core. Thus, emission can be ascribed to a phosphorescent process with a mixture of a MLCT from the Re(dπ) → NHC(π*), LLCT from the imidazolyl/pyridyl to the NHC ligand, and LC (NHC derivative) transitions. In all cases, the emission maximum is blue-shifted in comparison with that observed in the typical diimine-Re(I) systems. Only the heterobimetallic species displayed antiproliferative activity against tumor lung A549 cells, which was increased after irradiation at 405 nm up to nearly 5 times for complexes **4** and **5**. A necrotic process seems to be the preferred cell death mechanism. Fluorescence microscopy showed that only heterobimetallic complexes **4** and **5** were suitable for cell visualization. Their biodistribution pattern reveals accumulation within the cytoplasm close to the nucleus and some nucleus permeation. Overall it can be suggested that, whereas the emissive properties are dominated by the NHC-Re(I) fragment, the anticancer activity is mainly dependent on the Au(I) counterpart.

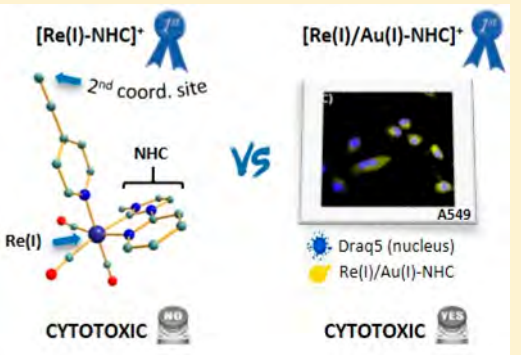

INTRODUCTION

Cancer is a disease that has been a leading cause of death in the past decade. For that reason, further research into new anticancer drugs is essential and one of the latest strategies to tackle this problem is to build bioactive trackable species.[1] The aim of this strategy is the compilation of information regarding the biodistribution and inner-interplay of drugs with the biological targets in order to design and deliver a sophisticated generation of anticancer metallodrugs. Within this framework several metallic structures combining well-known anticancer metal species such as cisplatin,[2] auranofin,[3] and RAPTA[4] analogues with either an organic chromophore or an emissive metallic species have already been described (see Figure 1A). However, a step forward would be the incorporation of an emissive species that is able to add extra antiproliferative value to the metallodrugs. Luminescent Re(I) complexes of the type *fac*-[Re(N^N)(CO)$_3$(X/L)]$^{+/0}$, where N^N represents a diimine derivative and X is a halogen or L an N-donor ligand, have been proven to be excellent cellular imaging agents for fluorescence microscopy.[5] Their emission is generally assigned to a ^{3}MLCT (metal to ligand charge transfer) transition, where the diimine is the main ligand contributor.[6] As consequence, L can be easily functionalized to introduce the bioactive fragment with no alterations of the emissive properties. In general, these types of Re(I) complexes do not seem to affect the antiproliferative properties when they are combined with a bioactive target (Figure 1B).[7] However, it was recently reported that the coordination of a bidentate N-heterocyclic carbene instead of the typical diimine ligand gives the Re(I) complex a remarkable anticancer activity against pancreatic cancer cells (see Figure 1B).[8] This was the first and the only example in which a Re(I) species containing a bidentate N-heterocyclic carbene has been tested as an anticancer agent, and on the basis of the promising result it seems clear that the substitution of the typical diimine ligand for a bidentate NHC scaffold has been key to achieve an anticancer rhenium drug. Alternatively antimicrobial activity was also recently found for rhenium complexes containing monodentate NHC ligands.[9] Therefore, it can be postulated that the combination of an NHC-Re(I) derivative with a metallodrug would be an excellent approach to maximize the therapeutic potential of a trackable metallodrug. Additionally, further substitution of L, which to the best of our knowledge has been only reported as a halogen for these types of Re(I) bidentate N-heterocyclic carbene derivatives[10] for a neutral N-donor ligand, will deliver high-potential mitochondrial bioprobes, as (1) cationic species present a greater predisposition to permeate those cellular membranes and (2) the N-donor ligand could be easily used as a linker to build the theranostic agents. Moreover, new

Received: August 20, 2018

DOI: 10.1021/acs.organomet.8b00601
Organometallics XXXX, XXX, XXX–XXX

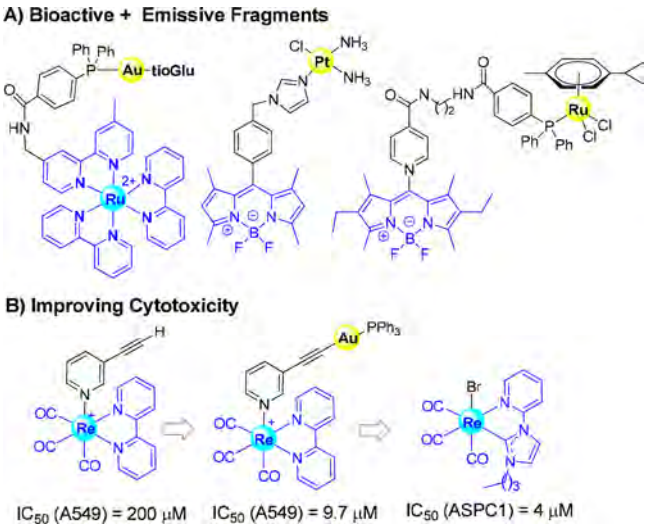

Figure 1. Examples of (A) the combination of bioactive and emissive fragments and (B) cytotoxicity displayed by either diimine or NHC-Re(I) derivatives.

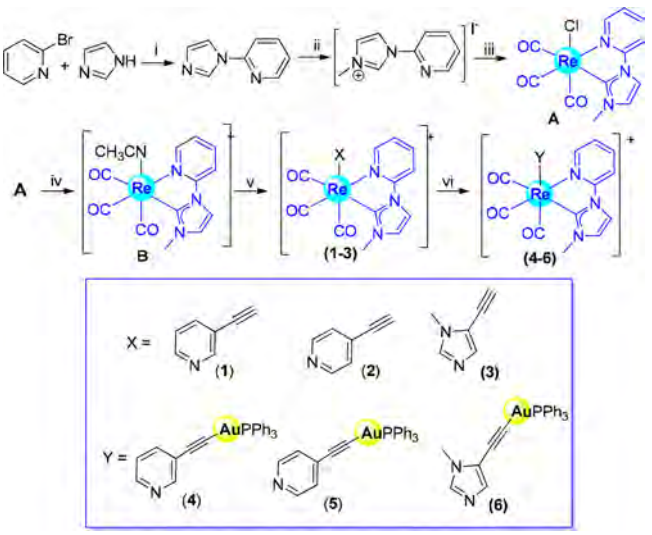

Figure 2. Schematic synthetic procedure and depiction of final complexes **1**–**6**. Legend: (i) K_2CO_3, 190 °C, 18 h; (ii) MeI, THF, room temperature, 24 h; (iii) Ag_2O, $Re(CO)_5Cl$, CH_3CN; (iv) AgOTf, CH_3CN, reflux 5 h; (v) alkynylpyridine derivative, THF, reflux; (vi) $Au(acac)PPh_3$, DCM.

grounds for the photophysical properties of these types of Re(I) complexes would be established. It is expected that their emissive behavior will differ from that seen for the reported neutral NHC-Re(I) complexes.[11]

Thus, herein we describe the first approach toward the use of luminescent N-heterocyclic carbene based Re(I) species as cell imaging agents as well as building blocks for trackable anticancer metallodrugs.

RESULTS AND DISCUSSION

Synthetic Approach. In previous studies we have validated the possibility of visualizing bioactive gold(I) complexes in cancer cells by a combination of the bioactive metallic fragment with a luminescent Re(I) species, using either functionalized alkynes or phosphines as linkers.[7] In the present work the focus is on the development of lumininescent heterobimetallic Re(I)/Au(I) complexes with an improved antiproliferative activity toward cancer cells. For that, substitution of the typical diimine ligand within the Re(I) scaffold by an analogous N-heterocyclic carbene (NHC) chelate is proposed. These systems would deliver the first example of a NHC-Re(I)/Au(I) heterobimetallic complex used for cellular imaging and as an anticancer agent. Similarly to previous synthetic procedures the *N*-methyl-*N*′-2-pyridylimidazolium salt was prepared by nucleophilic substitution of imidazole with 2-bromopyridine followed by an imidazole alkylation reaction with methyl iodide.[12] The *N*-methyl-*N*′-2-pyridylimidazolium salt reacts with silver oxide, forming the silver carbene that transmetalates in situ with $Re(CO)_5Cl$, in acetonitrile, to give **A** in a moderate yield (Figure 2).[13] It is worth noting that the presence of the chelated NHC within the *fac*-{$Re(I)CO_3$} core instead of the symmetric diimine ligand generates a pair of enantioners. Therefore, further modification of **A** leads to subsequent racemic mixtures. Afterward, abstraction of the chloride ligand by silver triflate in acetonitrile led to the activated Re(I)-NHC species **B**, which can be easily derivatized by further substitution of the labile acetonitrile ligand for the corresponding alkyne derivatives to give complexes **1**–**3**. In order to prepare the bimetallic Re(I)/Au(I) species, the Re(I) precursor was stirred in either DCM or acetonitrile in the presence of $Au(acac)PPh_3$. The acetylacetonate complex facilitates the deprotonation of the alkyne and the subsequent coordination of the gold atom to the triple bond, thus affording the bimetallic complexes **4**–**6**. All complexes have been characterized by ^1H, $^{13}C\{^1H\}$, $^{31}P\{^1H\}$ NMR, FT-IR, and UV–vis spectroscopy as well as mass spectrometry, corroborating the accomplishment of their synthesis. Analyses of the CO stretching frequencies of all the complexes corroborate the expected facial arrangements, as three stretches at ca. 2020, 1940, and ca. 1890 cm^{-1} for complexes **1**–**3** and two stretches for **4**–**6** at around 2022 and 1900 cm^{-1} are observed because of the overlap of A′(2) and A″ modes into a single broad band. Similar NHC-rhenium tricarbonyl derivatives presented analogous values.[14] Moreover, the heterobimetallic complexes lack a ν(H–C≡C) band, which had been observed for their Re(I) precursors, indicating the coordination of the gold fragment (see Table 1). Additionally, in all cases, ^1H NMR spectra were well-defined and showed the typical patterns for the *N*-methyl-*N*′-2-pyridylimidazolium and the corresponding pyridyl or imidazolyl carbene derivative coordinated to a *fac*-$Re(CO)_3$ core. Specifically, the disappearance of the acidic imidazolium

Table 1. IR Stretching Bands (cm^{-1}) and $^{31}P\{^1H\}$ and $^{13}C\{^1H\}$ NMR (ppm) Chemical Shifts (CD_2Cl_2) of 1–6

	IR ν(CO)	IR ν(H–C≡C)	$^{31}P\{^1H\}$ NMR	^{13}C NMR C≡C–H/Au
1	2022s, 1926m, 1895s	3238w		78.0[b]
2	2019s, 1955m,1908s	3236w		79.5
3	2023s, 1945m,1887s	3229w		69.2
4	2023s, 1900s,br		41.5	98.0
5	2021s, 1897br		41.5	99.2
6	2019s, 1893br		41.8	no

[a]Abbreviations: w, weak; m, medium; s, strong; br, broad; no, not observed. [b]CD_3CN.

DOI: 10.1021/acs.organomet.8b00601
Organometallics XXXX, XXX, XXX–XXX

Table 2. Relevant Bond Lengths (Å) and Angles (deg) of Complexes B, 1, and 3

complex B		complex 1		complex 3	
Re(1)−C(1)	1.911(5)	Re(1)−C(1)	1.968(4)	Re(1)−C(1)	1.921(4)
Re(1)−C(2)	1.972(6)	Re(1)−C(2)	1.911(4)	Re(1)−C(2)	1.968(6)
Re(1)−C(3)	1.906(6)	Re(1)−C(3)	1.935(4)	Re(1)−C(3)	1.906(4)
Re(1)−C(4)	2.125(5)	Re(1)−C(9)	2.130(4)	Re(1)−C(4)	2.135(6)
Re(1)−N(3)	2.202(4)	Re(1)−N(1)	2.212(3)	Re(1)−N(3)	2.192(4)
Re(1)−N(4)	2.144(5)	Re(1)−N(4)	2.225(3)	Re(1)−N(4)	2.188(3)
C(1)−O(1)	1.156(6)	C(1)−O(1)	1.144(4)	C(1)−O(1)	1.141(5)
C(2)−O(2)	1.140(7)	C(2)−O(2)	1.149(5)	C(2)−O(2)	1.146(7)
C(3)−O(3)	1.1569(7)	C(3)−O(3)	1.149(5)	C(3)−O(3)	1.155(6)
N(4)−Re(1)−C(3)	175.7(3)	N(4)−Re(1)−C(3)	178.7(1)	N(4)−Re(1)−C(3)	174.3(2)
C(4)−Re(1)−N(3)	74.6(2)	C(9)−Re(1)−N(1)	74.5(1)	C(9)−Re(1)−N(3)	74.9(2)

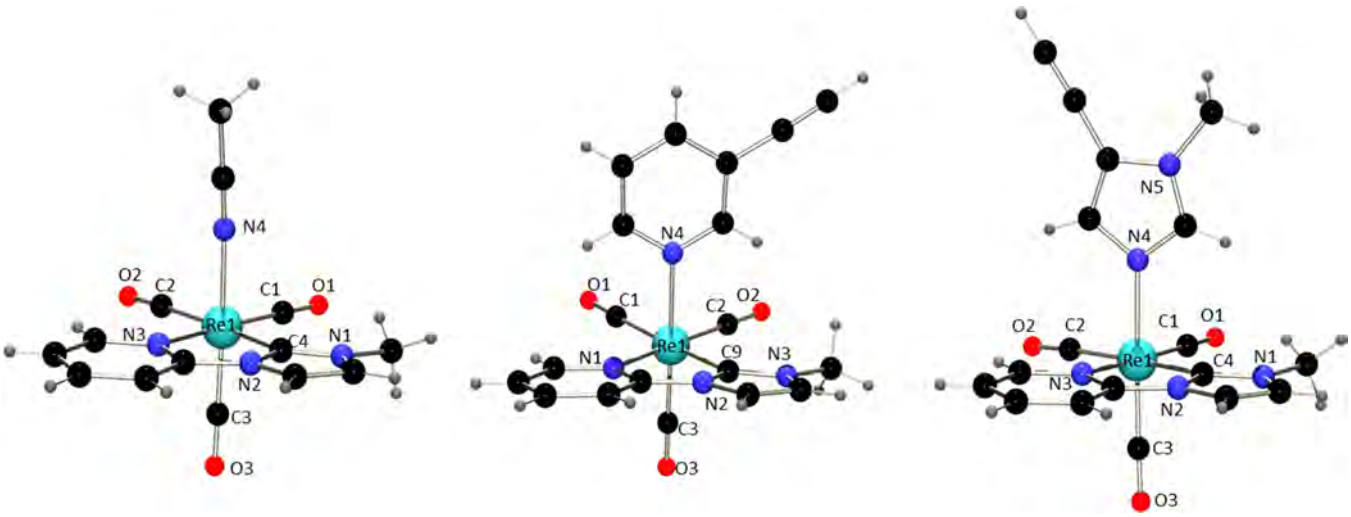

Figure 3. Pov-ray representations of complexes B, 1, and 3 (the triflate counterions are omitted for clarity). Note that the molecular representations of the complexes correspond to the same chirality.

proton signal in the 10−12 ppm region of the ^{1}H NMR spectrum was observed. Consequently, a new carbenoic carbon signal appears between 189 and 197 ppm in the ^{13}C NMR spectra together with the carbonyl carbons, confirming the coordination of NHC as a bidentate ligand to the rhenium core.[15] Moreover, as a result of the gold triphenylphosphine coordination, the heterobimetallic complexes **4**−**6** revealed in their ^{1}H NMR spectra a new multiplet resonance in the region between 7.49 and 7.55 ppm due to the presence of the new fragment, as well as the disappearance of the terminal alkyne protons present in their precursors at 3.70, 3.62, and 3.50 ppm, respectively, in concordance with the IR results. In addition to that, the downfield shift of the alkynyl carbons seen by ^{13}C NMR spectroscopy upon the coordination of −AuPPh$_3$ and the single peak at ca. 41 ppm observed by ^{31}P NMR spectroscopy are consistent with the values obtained for similar species.[7a] Further analytical data provided by mass spectrometry corroborated the accomplishment of the synthesis.

Crystal Structures. Complexes **B**, **1**, and **3** are chiral complexes and have been crystallized as racemic mixtures by slow diffusion of Et_2O in CH_2Cl_2 (**1**, **3**) or CH_3CN (**B**). Molecular structures together with selected bond distances and angles are presented in Table 2 and Figure 3. The three complexes presented a single molecule per asymmetric unit, and their space groups *Pn*, $P2_1/n$, and $P2_1/c$, respectively, are acentric, but not chiral, or centrosymmetric, and both enantiomers of each of the species can be observed in the crystal lattice (see Figure S1). In all cases, the rhenium coordination sphere could be described as a distorted octahedron, where the three carbonyls are arranged in a facial disposition. Thus, the NHC system lies on the equatorial plane together with two carbonyl ligands, whereas the remaining carbonyl and the corresponding N-donor ligand are located in the axial positions of the octahedron. The Re−$C_{carbene}$ distances are 2.125(5), 2.130(4), and 2.135(6) Å for complexes **B**, **1**, and **3**, respectively, which are very close to those values reported for similar carbene Re species.[16] Moreover, Re−CO bond distances trans to the NHC unit were much longer (ca. 1.970 Å) in comparison with the other Re−CO distances (ca. 1.915 Å) due to the well-known trans influence of NHC species. Consequently, we observed a shortening of the C−O bond length of the corresponding carbonyl trans to the NHC as a result of the lower π-back-bonding character from the metal to the carbonyl unit (see Table 2). These bond length differences are in agreement with the published crystallographic data of similar NHC-rhenium complexes.[11b] It is also worth mentioning that the NHC chelate provides a similar constriction to the complex in comparison to their analogous bipy[17] or phen[18] chelates, with narrow C−Re−N angles at ca. 74°, comparable to those of the cited bidentate ligands.

DOI: 10.1021/acs.organomet.8b00601
Organometallics XXXX, XXX, XXX−XXX

Optical Properties. The photophysical properties of complexes **1**−**6** were analyzed by UV−vis absorption and emission spectroscopy in dimethyl sulfoxide solution at room temperature. The most significant data are collected in Table 3,

Table 3. Photophysical Properties of 1−6 in Degassed DMSO Solution[a]

	λ_{abs}/nm (ε/L mol^{-1} cm^{-1})	λ_{em}/nm (λ_{em}/nm)	τ/ns
1	288 (14000), 320 (8000)	440, 460 (s) (400)	
2	291 (14800), 317 (10900)	456, 481 (s), 514 (413)	212
3	286 (10100), 323 (5800)	488 (370)	10, 136
4	285 (36700), 316 (14600)	460, 485 (s), 514 (414)	31, 205
5	288 (30300), 310 (28170)	465, 483 (s), 512 (412)	207
6	280 (25400), 339 (4000)	493 (377)	15, 123

[a]Aerated DMSO: τ(**2**) = 175 ns. Degassed DMSO: imidazolium salt: λ_{em} 440 nm (λ_{exc} 295 nm); **A**: λ_{em} 506 nm (λ_{exc} 401 nm). Abbreviation: s, strong.

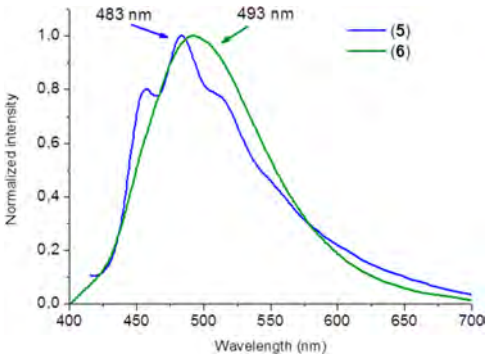

Figure 4. Emission spectra of complexes **5** and **6** in degassed DMSO at 298 K.

Figure 4, and Figures S2 and S3. All of the complexes showed a similar absorption pattern, with an intense absorption band at ca. 290 nm that can be attributed to $\pi \rightarrow \pi^*$ transitions within the NHC ligand and also within the phenyl groups in the case of the heterobimetallic complexes. Additionally, all of the complexes presented a lower energy band with relatively small molar absorptivity above 300 nm. This band could be attributed to a mixture of MLCT (Re → NHC) and LLCT (pyridyl/imidazolyl → NHC) transitions, and thus, it is best described as a MLLCT transition.[13,14] With regard to the emissive properties, these complexes presented blue-shifted emission maxima in comparison with those of the typical $[Re(CO)_3(N^N)L]^{0/+}$.[6] Such a blue shift is a result of the strongly σ donating NHC ligands, which ensure strong ligand fields with high-lying d−d excited states. Specifically complexes **1**, **2**, **4**, and **5** exhibit a structured emission at ca. 481 nm, whereas complexes **3** and **6** presented slightly red shifted broad emission bands at 488 and 490 nm, respectively (see Figure 4 and Figure S3). The fact that the imidazolyl derivatives **3** and **6** presented red-shifted emission maxima in comparison with their analogues **1**, **2**, **4**, and **5** species could be associated with the more highly electron donating character of the imidazole vs pyridyl derivative present in the axial position of the Re(I) metal center. In consequence, the HOMO orbitals, which are primarily located in the Re(I), become slightly destabilized and a red shift of the emission maximum is seen.[15a] The emissions could therefore be attributed to a MLLCT transition, i.e. an MLCT transition from Re(dπ) → NHC(π^*) mixed with an LLCT transition from the imidazolyl/pyridyl to the NHC ligand. In addition to that, it is also worth mentioning that the structured emission profile observed especially for complexes **1**, **2**, **4** and **5** suggests that the MLLCT could be partially mixed with a ^{3}LC state.[13] Demas and DeGraff already postulated such behavior in the cases where MLLCT and LC states were energetically similar.[19] The significant LC state contribution to the emission could also be deduced from the similarities between the excitation and emission profile of the imidazolium salt itself with that of the complexes (see Figure S3). Lifetime values at room temperature range from tens to hundreds of nanoseconds, which are typical of phosphorescent nature in this family of complexes.[15] Additionally, the presence of the gold fragment grafted in the axial ligand does not seem to affect the photophysical behavior of the species, which is in concordance with other heterobimetallic species reported.[7a]

Biological Properties. The cytotoxic activity of complexes **1**−**6** as well as their rhenium precursors **A** and **B** was determined by an MTT assay in the lung A549 tumor cell line (see Table 4). Only the heterobimetallic complexes presented

Table 4. IC_{50} Values of 1−6 in A549 Cells after Incubation for 24 h in the Absence of Light and after Irradiation for 10 min at 405 nm

	IC_{50}	IC_{50} (irradiated)
1	>50	>50
2	>50	>50
3	>50	>50
4	12.18 ± 1.19	4.48 ± 0.71
5	10.82 ± 1.63	2.66 ± 0.56
6	12.65 ± 2.10	9.97 ± 3.04
A	>50	>50
NHC	>50	>50

a significant antiproliferative character, ca. 11 μM. In contrast, the monometallic rhenium complexes showed cytotoxicity values of over 50 μM in all cases, which point toward the gold fragment as the bioactive entity for complexes **4**−**6**. As similar NHC rhenium derivatives have been proven to dissociate CO under photochemical conditions,[15b] complexes **A**, **B**, and **1**−**3** were tested as photocytotoxic agents using the same cell line. However, irradiation at 405 nm for 10 min did not showed the expected increase in toxicity. Once again, all of them presented IC_{50} values of over 50 μM. In addition to the monometallic species, the heterobimetallic complexes were also analyzed under photochemical conditions. All of them showed a slight improvement in their antiproliferative character (see Table 4), complex **6** being the least affected by application of the irradiation. Despite the promising result, these complexes could not be considered as effective photocytotoxic agents, as their level of toxicity in the absence of light is already high (ca. 11 μM). The cell death mechanism of heterobimetallic complexes was investigated by flow cytometry (see Figure S4). Complex **4** was incubated at different concentrations with A549 cells for 24 h. Annexin V-DY634 and 7-AAD were used as fluorescent markers. Annexin V-DY634 binds to phosphatidylserine in the cell membrane, and 7-AAD is a vital dye that only enters through a damaged cell membrane. Moreover, Z-VAD-fmk, a cell permeant pan caspase inhibitor, was used as an indicator of the participation of caspases in cell death. Since

DOI: 10.1021/acs.organomet.8b00601
Organometallics XXXX, XXX, XXX−XXX

the cells incubated with both markers seemed to have a positive response by flow cytometry together with the speed of cell death observed, it can be concluded that the cell death mechanism is likely to be by a necrotic process. Moreover, the fact that the cells incubated with Z-VAD-fmk behave in the same way that those lacking such a caspase inhibitor corroborates that the cellular death is following a pathway independent of caspases (see Figure S5). Additionally, a similar experiment was performed but this time with irradiation of the samples for 10 min at 405 nm during the incubation period in order to assess whether the irradiation process was somehow affecting the cellular death pathway. Once again the result was similar to that of the nonirradiated experiment; necrosis seems to be the preferred cellular death. Investigations regarding the biological targets for these complexes were also undertaken. Thus, inhibition of the thioredoxin reductase was performed using complex **4** as a model. Specifically, A549 cells were treated with complex **4** or vehicle (DMSO) for 4 h. Then, total protein extracts were prepared and used for the determination of thioredoxin activity. Thereafter, the artificial substrate 5,5′-dithiobis(2-nitrobenzoic acid) (DTNB) was added, which would rapidly evolve to two molecules of 2-nitro-5-thiobenzoate anion (TNB) if thioredoxin reductase is in the presence of NADPH. The reduction of DTNB to TNB affords a yellow color that can be detected at 412 nm by UV−vis absorption.[20] The evolution of the TNB formation was recorded for 5 min, and its comparison with that of a control assay did not show inhibition of the thioredoxin (see Figure 5).

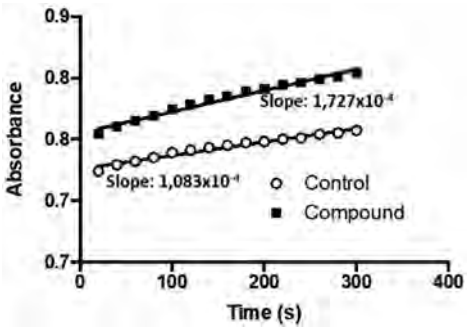

Figure 5. Inhibition of thioredoxin assay for complex **4**: representation of the evolution of absorbance intensity of TNB over 5 min.

This result was further confirmed by a preliminary analysis of the production of reactive oxygen species (ROS) in colorectal adenocarcinoma cells (CACO cells). Once again, incubation of complex **4** with CACO cells did not promote the production of ROS, which suggests a biological target different from that of thioredoxin.

In an attempt to elucidate the biodistribution of complexes **1**−**6**, fluorescence microscopy was used. The species were incubated with A549 cells for 24 h at a concentration lower than their IC_{50} value in order to prevent cell death during the experiment. In addition, Draq5, a nuclear dye with an excitation wavelength of 647 nm, was used as an internal standard to ascertain their localization. Cellular images were taken after exciting the cells at 405 nm, where the emissive complexes could be visualized. Superimposition of those images with the corresponding images taken after exciting the samples at 647 nm allowed elucidation of whether the complexes **1**−**6** were within the cell and/or inside the nucleus. Unexpectedly, none of the monometallic rhenium complexes were visible within this assay. In contrast, two out of the three heterobimetallic complexes showed emission within the cytoplasm surrounding the nucleus and in a smaller amount inside the nucleus (Figures 6 and 7). Specifically, **4** and **5** were

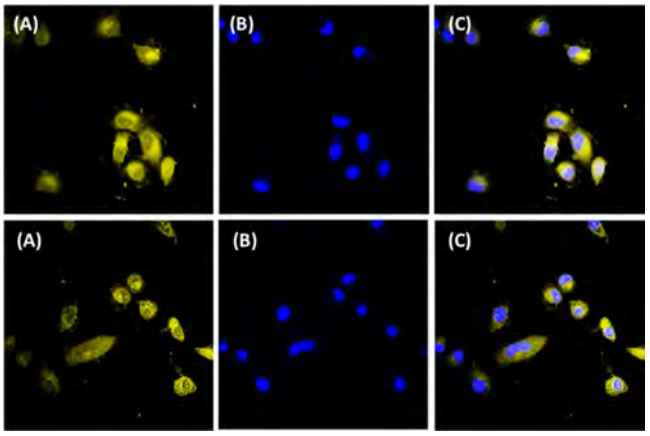

Figure 6. Images of complexes **4** (top row) and **5** (bottom row) incubated with A459 cells and Draq5 at 37 C for 4 h: (A) after irradiation at 405 nm; (B) after irradiation at 647 nm; (C) superimposed image.

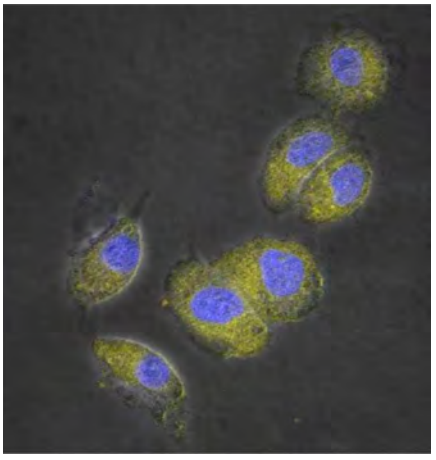

Figure 7. Image of complex **5** (yellow color) incubated with A459 cells and Draq5 (blue color) at 37 C for 4 h superimposed with the bright field image.

the complexes that were able to be visualized within the cell. A closer look at other heterobimetallic Re(I)/Au(I) complexes reported in the literature as possible cell visualization or theranostic agents indicates that typically those containing in their structure the fragment $AuPPh_3$ appear to have more permeability in comparison to their monometallic rhenium analogues.[7] The present case seems to follow the same trend except for complex **6**, which despite having a $-AuPPh_3$ fragment was not observable. A plausible explanation for this result might relay on the photophysical properties of complex **6**. In contrast to complexes **4** and **5**, whose maximum excitation wavelengths were at around 410 nm in both cases, in complex **6** the maximum excitation was at 377 nm (see Table 3 and Figure S3). Therefore, irradiation of the cells at 405 nm would not be suitable to excite complex **6**, and consequently emission would not be observed. This result is in line with the lower photocytotoxicity seen in the case of complex **6** in

DOI: 10.1021/acs.organomet.8b00601
Organometallics XXXX, XXX, XXX−XXX

comparison with complexes **4** and **5** (see Table 4). It is possible that the irradiation used is not equally effective.

As previously commented, complexes **1**−**3** were not suitable for cell imaging within these conditions. To assess whether a possible disruption of the molecules under biological conditions was taking place, thus preventing their visualization, a stability assay was performed. Specifically, complexes **1** and **4** were chosen as representative species and they were dissolved in a mixture of DMSO and PBS (<0.5% DMSO). The stability of the complexes was analyzed by UV−vis absorption spectroscopy over a period of 24 h. Both complexes seemed to remain stable under those conditions (see Figure S6). Therefore, it seems clear that decomposition of the complexes could not be the origin of the lack of response in the localization experiment for the monometallic species **1**−**3**. The main difference between these Re(I) species and those already studied by fluorescence microscopy is the nature of the chelated ligand.[21] Thus, changing the typical diimine ligand for a pyridyl-carbene derivative (NHC) seems to negatively affect the internalization process.

CONCLUSIONS

In summary, the first bioactive and luminescent heterobimetallic Re(I)/Au(I) complexes containing a pyridyl N-heterocyclic carbene derivative instead of the typical diimine ligand were reported, as well as their monometallic Re(I) precursors. Either pyridyl or imidazolyl alkyne derivatives were used as bridging ligands between both metals, being specifically bonded to the Re(I) center through the nitrogen atom and to the Au(I) center through the alkynyl carbon. The photophysical properties of these complexes showed that all of them have a similar behavior, where the presence of the Au(I) fragment was not implicated in the emissive process. Thus, the emission was attributed to a mixture of ^{3}MLCT from Re(dπ) → NHC(π*) and ^{3}LLCT from the imidazolyl/pyridyl to the NHC ligand as well as ^{3}LC (NHC derivative) transitions. The similar structured emission profiles seen for NHC, **1**, **2**, **4**, and **5** was conclusive on the implication of LC transitions. Moreover, such an LC contribution seems to be less marked in the case of complexes with axial ligands such as a chloride (**A**) or imidazolyl derivatives (**3** and **6**), whose electron-donating character is higher, and presumably the contribution of the LLCT over the LC transition as well. As expected, only the heterobimetallic complexes showed antiproliferative character against A549 cells (IC_{50} ≈ 11 μM). Therefore, at this point it can be stated that we have developed heterobimetallic species able to combine their intrinsic emissive (Re(I) fragment) and bioactive (Au(I) fragment) properties into a single new molecular structure. Additionally, irradiation of the cells incubated with the heterobimetallic complexes at 405 nm incremented the cytotoxicity up to 5 times in some cases. In contrast, monometallic Re(I) species did not show any extra antiproliferative activity. The cell death mechanism studied by flow cytometry concluded that a necrotic process seems to take place for the irradiated and nonirradiated assays. Moreover, fluorescence microscopy analysis showed that only **4** and **5** were able to accumulate within the cells. Specifically, their emission was within the cytoplasm surrounding the nucleus and in a smaller amount inside the nucleus. The fact that none of the monometallic Re complexes were detected by this technique could be a combination of several factors. Photophysical (lower intensity or quenching processes in the biological media) and/or the different lipophilic properties (lack of the gold triphenyl fragment and the presence of a pyridyl-NHC derivative instead of the typical diimine) could be implicated. Additionally, the different photophysical properties seem to be the origin for the inability to detect **6** by fluorescence microscopy. In this particular case we believe that it is possible that the complexes have entered the cells, as it is known that the fragment $AuPPh_3$ renders a higher lipophilicity of the probe and, thus, a better cell permeability. However, this complex has a maximum excitation wavelength of ca. 370 nm, which is quite far from the excitation wavelength used within the visualization experiment (405 nm).

To conclude, the development of heterobimetallic Re(I)/Au(I) complexes as emissive and bioactive species could be achieved on attending to the different functionalizations of (a) the chelate ligand NHC to modulate the desired photophysical properties and (b) the bridging and ancillary gold ligands in order to endow specific bioactivity.

EXPERIMENTAL SECTION

General Measurements and Analysis Instrumentation. Mass spectra were recorded on a Bruker Esquire 3000 Plus instrument, with the electrospray (ESI) technique, and on a Bruker MALDI-TOF instrument. ^{1}H, ^{13}C{^{1}H}, and ^{31}P{^{1}H} NMR, including 2D experiments, were recorded at room temperature on a Bruker Avance 400 spectrometer (^{1}H, 400 MHz; ^{13}C, 100.6 MHz; ^{31}P, 162 MHz) with chemical shifts (δ, ppm) reported relative to the solvent peaks of the deuterated solvent. Infrared spectra were recorded in the range 4000−250 cm^{-1} on a PerkinElmer Spectrum 100 FTIR spectrometer. Room-temperature steady-state emission and excitation spectra were recorded with a Jobin-Yvon-Horiba Fluorolog FL3-11 spectrometer fitted with a JY TBX picosecond detection module. Nanosecond lifetimes were recorded with a Datastation HUB-B apparatus with a nanoLED controller and DAS6 software. The nanoLEDs employed for lifetime measurements had wavelengths of 370 and 390 nm. The lifetime data were fitted using the Jobin-Yvon software package and the Origin Pro 8 program. UV−vis spectra were recorded with 1 cm quartz cells on an Evolution 600 spectrophotometer. The quantum yields were measured in a Hamamatsu Photonics Quantaurus-QY instrument at 300−950 nm.

Crystal Structure Determinations. Crystals were mounted in inert oil on glass fibers and transferred to the cold gas stream of an Oxford Diffraction Xcalibur diffractometer equipped with a low-temperature attachment. Data were collected using monochromated Mo Kα radiation (λ= 0.71073 Å), with scan type ω. Absorption corrections based on multiple scans were applied using spherical harmonics implemented in the SCALE3 ABSPACK scaling algorithm. The structures were solved by direct methods and refined on F^2 using the program SHELXL-97.[22] All non-hydrogen atoms were refined anisotropically, with the exception of complex **7**. CCDC deposition numbers 1858777 (**B**), 1858778 (**1**), and 1858779 (**3**) contain the supplementary crystallographic data. These data can be obtained free of charge from the Cambridge Crystallography Data Center.

Antiproliferative Studies: MTT Assay. Exponentially growing cells (A549) were seeded at a density of approximately 10^4 cells per well in 96-well flat-bottomed microplates and allowed to attach for 24 h prior to addition of the compounds. The complexes were dissolved in DMSO and added to cells in concentrations ranging from 10 to 200 μM in quadruplicate. Cells were incubated with our compounds for 24 h at 37 °C. A 10 μL portion of MTT (5 mg mL^{-1}) was added to each well, and the plates were incubated for 2 h at 37 °C. Finally, the growth medium was eliminated and DMSO (100 μL per well) was added to dissolve the formazan precipitates. The optical density was measured at 550 nm using a 96-well multiscanner autoreader (ELISA). The IC_{50} values were calculated by nonlinear regression analysis.

DOI: 10.1021/acs.organomet.8b00601
Organometallics XXXX, XXX, XXX−XXX

Flow Cytometry Assay. The cells were treated for 24 h with compound **4** at 5, 10, and 25 μM. Then, they were trypsinized and incubated at 37 °C for 5 min in ABB (140 mM NaCl, 2.5 mM $CaCl_2$, 10 mM Hepes/NaOH, pH 7.4) containing 0.5 mg mL^{-1} of either annexin V-DY634 or 7-AAD. Finally, the cells were diluted to 0.5 mL with ABB and analyzed by flow cytometry (FACScan, BD Biosciences, Spain).

Thioredoxin Inhibition Assay. For determination of the thioredoxin reductase activity, A549 cells were incubated for 9 h with our compounds at different concentrations near the IC_{50} values. Cells were collected, washed with PBS and 150 μL of buffer (1% Triton X-100, 150 mM NaCl, 50 mM Tris/HCl pH 7.6, 10% v/v glycerol, 1 mM EDTA, 1 mM sodium orthovanadate, 10 mM sodium pyrophosphate, 10 μg mL^{-1} leupeptin, 10 mM NaF, 1 mM sodium methylsulfonium) for 30 min at 0 °C, and centrifuged at 200*g* for 10 min at 4 °C. The protein was quantified using the BCA protein assay (Thermo Scientific), and 80 μg was added in each assay. Kinetic studies were performed in a buffer containing 0.2 M NaCl, H-phosphate pH 7.4, 2 mM EDTA, 0.25 mM NADPH, and 3 mM DTNB. The increase in the absorbance was measured at 412 nm for 5 min at 25 °C.

Intracellular Peroxide (ROS) Formation. The production of ROS (reactive oxygen species) was assessed using the dichlorofluorescein (DCF) assay.[23] Caco-2/TC7 cells were plated in 96-well plates at a density of 4000 cells per well and incubated for 24 h under standard cell culture conditions. For treatment, **4** was added to cells within its IC_{50} concentration and incubated for 24 h; mock treated cells were just incubated with DMSO at the same concentration as for treated cells. Then, cells were washed twice with PBS and 100 μL of 20 mM DCFH-DA (dichlorodihydrofluorescein diacetate) was added to each well. Cells were incubated for 1 h at 37 °C and washed twice with PBS; finally, 100 μL of PBS was added and the fluorescence was analyzed with DTX-880 (Beckman Counter). Excitation and emission settings were 485 and 535 nm, respectively. The intensity of fluorescence is considered a reflection of total intracellular ROS.

Cell Fluorescence Microscopy Study. Cells from the European Collection of Cell Cultures were maintained in Hepes-modified minimum essential medium (DMEM) supplemented with 5% fetal bovine serum, penicillin, and streptomycin. A549 cells were detached from the plastic flask using trypsin-EDTA solution and suspended in an excess volume of growth medium. The homogeneous cell suspension was then distributed into 24-well flat-bottomed microplates over a cover slip placed inside each well, and they were allowed to attach for 24 h prior to addition of compounds. Complexes were added (10 μL) to the cells up to a final concentration of 25 μM. After incubation for 4 h at 37 °C, the growth medium was removed and 0.5 mL of PBS was added for a washing step (three times). Thereafter, 0.5 mL of paraformaldehyde (4%) was added and the plates were allowed to stand for 15 min at room temperature. Eventually the paraformaldehyde was removed and further washings with PBS were performed (3 × 0.5 mL). The cover slips were collected from the 24-well plate, immersed for 1 or 2 s in distilled water, and left in order to allow the water to drip off. Then, they were placed over a microscope slide where a drop of Fluoromount with 2 μM DRAQ5 had been previously placed. Preparations were viewed using an Olympus FV10-i Oil type compact confocal laser microscope using a ×10 or ×60 objective, with excitation wavelengths at 405 and 650 nm.

Materials and Procedures. The starting materials *N*-methyl-*N*′-2-pyridylimidazolium,[12] Au(acac)(PPh_3),[24] and complex **A**[13] were prepared according to literature procedures, and their experimental data agree with those reported elsewhere. All other starting materials and solvents were purchased from commercial suppliers and used as received unless otherwise stated.

Synthesis of Complex B. To a stirred solution of **A** (83 mg, 0.178 mmol) in CH_3CN (20 mL) was added AgOTf (50.4 mg, 0.196 mmol), and the mixture was refluxed over 5 h 30 min in the dark. The suspension was filtered over Celite and the solvent reduced to minimum volume. The addition of cold ether afforded an oil that after trituration gave the product as a pale yellow solid (yield 83 mg, 79%). ^{1}H NMR (400 MHz, CD_2Cl_2): δ 8.76 (ddd, J = 5.6, 1.6, 0.7 Hz, 1H, H_6), 8.25 (ddd, J = 8.4, 7.6, 1.6 Hz, 1H, H_4), 8.14 (d, J = 2.2 Hz, 1H, H_8 or H_9), 8.13−8.10 (ddd, J = 8.4, 1.2, 0.7 Hz, 1H, H_3), 7.44 (ddd, J = 7.5, 5.6, 1.2 Hz, 1H, H_5), 7.29 (d, J = 2.2 Hz, 1H, H_8 or H_9). ^{13}C NMR (101 MHz, CD_2Cl_2): δ 195.0 (s, CO), 194.7 (s, CO), 189.2 (s, CO), 187.0 (s, C_7), 154.3 (s, C_2), 153.8 (s, C_6), 143.7 (s, C_4), 125.8 (s, C_8 or C_9), 124.8 (s, C_5), 118.90 (s, C_8 or C_9), 114.32 (s, C_3), 39.78 (s, C_{10}), 4.32 (s, C_{12}). HRMS (m/z): 471.0470 [M − OTf], calcd for $C_{14}H_{12}N_4O_3Re$ 471.0462. IR (ν, cm^{-1}): 3155 (C_{Ar}−H), 2027, 1882 (CO), 1621 (C_{Ar}=N)

General Procedure for Coordination Synthesis of 1−3. To a stirred solution of **B** in THF was added the corresponding alkynylpyridine ligand, and the reaction mixture was heated for several hours until consumption of the starting material. The solvent was then evaporated and the crude mixture redissolved in DCM. Filtration over Celite followed by addition of ether afforded the desired product as a pale yellow solid.

Synthesis of Complex 1. Complex **B** (30 mg, 0.048 mmol) and 3-ethynylpyridine (25 mg, 0.242 mmol) were reacted in THF (5 mL) at 40 °C over 32 h (yield 23.7 mg, 72%). ^{1}H NMR (400 MHz, CD_3CN): δ 8.99 (d, J = 5.6 Hz, 1H, H_6), 8.39 (d, J = 1.7 Hz, 1H, H_{15}), 8.26−8.20 (m, 2H, H_4 + H_{11}), 7.93−7.89 (dt_{ap}, J = 8.0, 1.6 Hz, 1H, H_{13}), 7.89 (d, J = 2.2 Hz, 1H, H_9/H_8), 7.85 (dm, J = 8.4 Hz, 1H, H_3), 7.52 (ddd, J = 7.5, 5.6, 1.1 Hz, 1H, H_5), 7.39 (d, J = 2.2 Hz, 1H, H_9/H_8), 7.29 (ddd, J = 8.0, 5.7, 0.6 Hz, 1H, H_{12}), 4.10 (s, 3H, H_{10}), 3.70 (s, 1H, H_{17}). ^{13}C NMR (101 MHz, CD_3CN): δ 197.6 (s, CO), 191.3 (s, CO), 190.3 (s, C_7), 157.1 (s, C_{15}), 154.8 (s, C_{11}), 154.7 (s, C_6), 154.6 (s, C_2), 144.1 (s, C_4), 143.0 (s, C_{13}), 127.3 (s, C_{12}), 126.7 (s, C_9), 125.8 (s, C_5), 123.0 (s, C_{14}), 119.0 (s, C_8), 114.5 (s, C_{13}), 84.8 (s, C_{17}, (*C*C-H)), 78.0 (s, C_{16}, (*C*C−H)), 39.9 (s, C_{10}). HRMS (m/z): 533.0620 [M − OTf], calcd for $C_{19}H_{14}AuN_4O_3Re$ 533.0618. IR (ν, cm^{-1}): 3238 (CC−H), 3238 (C_{Ar}−H), 2113 (C≡C), 2022, 1926, 1895 (CO), 1618 (C_{Ar}=N).

Synthesis of Complex 2. 4-Ethynylpyridine hydrochloride (85 mg, 0.609 mmol) was dissolved in a saturated aqueous solution of $NaHCO_3$ and extracted with DCM. The organic phase was dried with anhydrous sodium sulfate and the solvent evaporated to dryness to afford 4-ethynylpyridine. Then the alkynylpyridine was reacted with complex **B** following the same procedure described for complex **1** (30 mg, 0.0484 mmol) in THF (5 mL) (yield 29.2 mg, 88%). ^{1}H NMR (400 MHz, CD_2Cl_2): δ 8.88 (ddd, J = 5.6, 1.6, 0.7 Hz, 1H, H_6), 8.26 (ddd, J = 8.4, 7.5, 1.7 Hz, 1H, H_4), 8.21 (dd, J = 5.1, 1.5 Hz, 2H, H_{11}), 8.19 (d, J = 2.2 Hz, 1H, H_9), 8.16 (ddd, J = 8.4, 1.7, 1.2 Hz 1H, H_3), 7.50 (ddd, J = 7.5, 5.6, 1.2 Hz, 1H, H_5), 7.35 (d, J = 2.2 Hz, 1H, H_8), 7.33 (dd, J = 5.1, 1.5 Hz, 2H, H_{12}), 4.12 (s, 3H, H_{10}), 3.62 (s, 1H, H_{15}). ^{13}C NMR (101 MHz, CD_2Cl_2): δ 197.4 (s, CO), 197.0 (s, CO), 190.3 (s, CO or C_7), 190.3 (s, CO or C_7), 154.1 (s, C_{12}), 154.1 (s, C_2), 153.8 (s, C_6), 144.1 (s, C_4), 134.2 (s, C_{13}), 129.7 (s, C_{12}), 126.3 (s, C_9), 125.6 (s, C_3), 119.1 (s, C_8), 114.7 (s, C_5), 87.6 (s, C_{15}, (CC-H)), 79.5 (s, C_{14}, (CC−H)), 39.8 (s, C_{10}). HRMS (m/z): 533.0644 [M − OTf], calcd for $C_{19}H_{14}AuN_4O_3Re$ 533.0618. IR (ν, cm^{-1}): 3236 (CC−H), 3236 (C_{Ar}−H), 2117 (C≡C), 2019, 1955, 1908 (CO), 1620 (C_{Ar}=N).

Synthesis of Complex 3. Complex **B** (56.6 mg, 0.091 mmol) and 5-ethynyl-1-methyl-1*H*-imidazole (9.6 μL, 0.091 mmol) were reacted in THF (5 mL) at 40 °C for 24 h. Purification was carried out by recrystallization in acetone/ether (yield 23.1 mg, 70%). ^{1}H NMR (400 MHz, CD_2Cl_2): δ 8.81 (ddd, J = 5.6, 1.6, 0.6 Hz, 1H, H_6), 8.20 (ddd, J = 8.4, 7.6, 1.6 Hz, 1H, H_4), 8.07 (d, J = 2.2 Hz, 1H, H_8), 8.03 (ddd, J = 8.4, 1.1, 0.6 Hz, 1H, H_3), 7.42 (ddd, J = 7.5, 5.6, 1.1 Hz, 1H, H_5), 7.32 (d, J = 2.2 Hz, 1H, H_9), 7.30 (s_{ap}, 1H, H_{16}), 6.96 (d, J = 1.3 Hz, 1H, H_{11}), 4.06 (s, 4H, H_{10}), 3.59 (s, 3H, H_{15}), 3.56 (s, 1H, H_{14}). ^{13}C NMR (101 MHz, CD_2Cl_2): δ 197.4 (s, CO), 197.1 (s, CO), 190.8 (s, CO or C_7), 189.7 (s, CO or C_7), 153.9 (s, C_2), 153.5 (s, C_6), 143.4 (s, C_4), 142.6 (s, C_{16}), 136.8 (s, C_{11}), 126.0 (s, C_9), 125.1 (s, C_5), 118.7 (s, C_8), 118.2 (s, C_{12}), 114.4 (s, C_3), 87.2 (s, C_{14}, (CC-H)), 69.2 (s, C_{13}, (*C*C−H)), 39.9 (s, C_{10}), 33.6 (s, C_{15}). HRMS (m/z): 536.0738 [M − OTf], calcd for $C_{18}H_{15}N_5O_3Re$ 536.0727. IR (ν, cm^{-1}): 3229 (CC−H), 3129 (C_{Ar}−H), 2125 (C≡C), 2023, 1945, 1887 (CO), υ 1617 (C_{Ar}=N).

DOI: 10.1021/acs.organomet.8b00601
Organometallics XXXX, XXX, XXX−XXX

General Procedure for Gold Addition. To a stirred solution of the rhenium precursor (**1**, **2** , or **3**) in acetonitrile or dichloromethane (5 mL) was added Au(acac)PPh_3. After 5 h of stirring at room temperature in the dark, the solution was filtered over Celite and concentrated to dryness. The solid was redissolved in DCM, and addition of ether afforded the desired product as a solid.

Synthesis of Complex ***4***. Complex **4** was obtained by following the general procedure for gold addition. Specifically, compound **1** (58 mg, 0.085 mmol) and Au(acac)PPh_3 (47.5 mg, 0.085 mmol) were stirred in DCM (5 mL), affording the desired product as an orange solid (yield 32.6 mg, 34%). ^{1}H NMR (400 MHz, CD_2Cl_2): δ 8.89 (dd, J = 5.6, 1.6 Hz, 1H, H_6), 8.37−8.36 (m, 1H, H_{14}), 8.26 (ddd, J = 8.5, 7.6, 1.6 Hz, 1H, H_4), 8.21 (d, J = 2.2 Hz, 1H, H_8), 8.17 (d_{br}, J = 8.4 Hz, 1H, H_3), 7.87 (dd, J = 5.6, 1.4 Hz, 1H, H_{11}), 7.76 (dd, J = 8.0, 1.4 Hz, 1H, H_{13}), 7.60−7.46 (m, 20H, H_{Ar}+H_5), 7.34 (d, J = 2.2 Hz, 1H, H_9), 7.16 (ddd, J = 8.0, 5.7, 0.6 Hz, 1H, H_{12}), 4.13 (s, 3H, H_{10}). ^{13}C NMR (101 MHz, CD_2Cl_2): δ 197.6 (s, CO), 197.1 (s, CO), 190.6 (s, C_7), 190.2 (s, CO), 157.0 (s, C_{14}), 154.1 (s, C_2), 153.4 (s, C_6), 150.6 (s, C_{11}), 144.1 (s, C_4), 142.3 (s, C_{13}), 134.8 (d,$^2J_{P-C}$ = 13.8 Hz, 6C, *o*-C, Ph), 132.4 (d, $^4J_{P-C}$ = 2.2 Hz, 3C, *p*-C, Ph), 129.9 (d, $^1J_{P-C}$ = 56.3 Hz, 3C, *i*-C, Ph), 129.9 (d, $^2J_{P-C}$ = 11.4 Hz, 6C, *m*-C, Ph), 126.7 (s, C_{12}), 126.5 (s, C_{15}), 126.2 (s, C_9), 125.51 (s, C_5), 119.2 (s, C_8), 98.0 (brs, C_{16}, (CC−H)), 114.7 (s, C_3), 39.8 (s, C_{10}). C_{17} (CC-Au) no observed. ^{31}P NMR (162 MHz, CD_3CN): δ 41.49. HRMS (m/z): 991.1122 [M − OTf], calcd for $C_{37}H_{28}AuN_4O_3PRe$ 991.1118. IR (ν, cm^{-1}): 3124 (C_{Ar}−H), 2125 (C≡C), 2023, 1900 (CO), 1617 (C_{Ar}=N).

Synthesis of Complex ***5***. Complex **5** was obtained by following the general procedure for gold addition. Specifically, compound **2** (30 mg, 0.044 mmol) and Au(acac)PPh_3 (24.6 mg, 0.044 mmol) were stirred in acetonitrile (5 mL), affording the desired product as a red solid (yield 31.2 mg, 62%). ^{1}H NMR (400 MHz, CD_2Cl_2): δ 8.89 (dd, J = 5.6, 0.9 Hz, 1H, H_6), 8.37−8.35 (m, 1H, H_{14}), 8.29−8.23 (m, 1H, H_4), 8.21 (d, J = 2.2 Hz, 1H, H_8), 8.17 (dm, J = 8.3 Hz, 1H, H_3), 7.88−7.85 (dm, J = 5.7 Hz, 1H, H_{11}), 7.76 (dm, J = 8.0 Hz, 1H, H_{13}), 7.61−7.46 (m, 15H, H_{Ar}), 7.34 (d, J = 2.2 Hz, 1H, H_9), 7.17 (ddd, J = 8.0, 5.7, 0.7 Hz, 1H, H_{12}), 4.13 (s, 3H, H_{10}). ^{13}C NMR (101 MHz, CD_2Cl_2): δ 197.7 (s, CO), 197.2 (s, CO), 190.6 (s, C_7), 190.5 (s, CO), 154.1 (s, C_6), 153.3 (s, 3C, C_{11}+C_2), 144.0 (s, C_4), 137.5 (s, C_{13}), 134.7 (d, $^2J_{P-C}$ = 13.8 Hz, 6C, *o*-C, Ph), 132.35 (d, $^4J_{P-C}$ = 2.4 Hz, 3C, *p*-C, Ph), 129.8 (d, $^3J_{P-C}$ = 11.4 Hz, 6C, *m*-C, Ph), 129.7 (d, $^1J_{P-C}$ = 56.9 Hz, 3C, *i*-C, Ph), 129.7 (s, 2C, C_{12}), 126.2 (s, C_9), 125.4 (s, C_3), 119.2 (s, C_8), 114.6 (s, C_5), 99.2 (br s, $C_{14,}$ (CC−Au)), 39.8 (s, C_{10}). C_{15}(CC-Au) not observed. ^{31}P NMR (162 MHz, CD_3CN): δ 41.49. HRMS (m/z): 991.1121 [M − OTf], calcd for $C_{37}H_{28}AuN_4O_3PRe$ 991.1118. IR (ν, cm^{-1}): 3124 (C_{Ar}−H), υ 2117 (C≡C), 2021, 1897 (CO), υ 1602 (C_{Ar}=N).

Synthesis of Complex ***6***. Complex **6** was obtained following the general procedure for the gold addition. Specifically, compound **3** (1 equiv, 17.8 mg, 0.026 mmol) and Au(acac)PPh_3 (1 equiv, 14.6 mg, 0.026 mmol) were stirred in acetonitrile (5 mL), affording the desired product as a beige solid (yield 16.8 mg, 52%). ^{1}H NMR (300 MHz, CD_2Cl_2): δ 8.81 (ddd, J = 5.6, 1.6, 0.7 Hz, 1H, H_6), 8.20 (ddd, J = 8.4, 7.6, 1.7 Hz, 1H, H_4), 8.09 (d, J = 2.2 Hz, 1H, H_8), 8.04 (ddd, J = 8.4, 1.2, 0.7 Hz, 1H, H_3), 7.60−7.45 (m, 16H, H_{Ar}), 7.41 (ddd, J = 7.5, 5.6, 1.2 Hz, 1H, H_5), 7.31 (d, J = 2.2 Hz, 1H, H_9), 7.15 (d, J = 1.4 Hz, 1H, H_{11}), 6.59 (d, J = 1.4 Hz, 1H, H_{12}), 4.06 (s, 3H, H_{10}), 3.57 (s, 3H, H_{14}). ^{13}C NMR (75 MHz, CD_2Cl_2): δ 197.5 (s, CO), 190.1 (s, CO or C_7), 153.8 (s, C_2), 153.5 (s, C_6), 143.4 (s, C_4), 140.6 (s, C_{11}), 134.74 (d, ^2J = 14.4 Hz, 6C, *o*-C, Ph), 133.93 (s, C_{12}), 132.35 (s, *p*-C, Ph), 129.86 (d, $^1J_{P-C}$ = 57.3 Hz, 3C, *i*-C, Ph), 129.73 (d, $^3J_{P-C}$ = 12.0 Hz, 6C, *m*-C, Ph), 125.94 (s, C_9), 125.00 (s, C_5), 120.97 (s, C_{13}), 118.64 (s, C_8), 114.16 (s, C_3), 39.81 (s, C_2), 33.25 (s, C_2). HRMS (m/z): 994.1238 [M − OTf], calcd for $C_{36}H_{29}AuN_5O_3PRe$ 994.1227. IR (ν, cm^{-1}): 3127 (C_{Ar}−H), 2019, 1893 (CO), 1617 (C_{Ar}=N).

■ ASSOCIATED CONTENT

Ⓢ Supporting Information

The Supporting Information is available free of charge on the ACS Publications website at DOI: 10.1021/acs.organomet.8b00601.

UV−vis absorption spectra of **1**−**6** in DMSO solution (5 × 10^{-5} M), normalized excitation and emission spectra of complexes **1**−**6**, imidazolium salt, and **A** in DMSO solution at 298 K, flow cytometry diagram of complex **4** incubated with A549 cells at different concentrations, incubation of A549 with complex **4** in the presence and absence of Z-VAD-fmk, a caspase inhibitor, superposition of UV−vis absorption graphs of complex **1** (5 × 10^{-5} M DMSO/PBS, <0.5% DMSO) taken over a period of 24 h, and superposition of UV−vis absorption graphs of complex **4** (5 × 10^{-5} M DMSO/PBS, <0.5% DMSO) taken over a period of 24 h (PDF)

Accession Codes

CCDC 1858777−1858779 contain the supplementary crystallographic data for this paper. These data can be obtained free of charge via www.ccdc.cam.ac.uk/data_request/cif, or by emailing data_request@ccdc.cam.ac.uk, or by contacting The Cambridge Crystallographic Data Centre, 12 Union Road, Cambridge CB2 1EZ, UK; fax: +44 1223 336033.

■ AUTHOR INFORMATION

Corresponding Authors

*E-mail for V.F-M.: vanesa@unizar.es.

*E-mail for M.C.G.: gimeno@unizar.es.

ORCID

Vanesa Fernández-Moreira: 0000-0002-1218-7218

M. Concepción Gimeno: 0000-0003-0553-0695

Notes

The authors declare no competing financial interest.

■ ACKNOWLEDGMENTS

This work is dedicated to Professor Ernesto Carmona in recognition of his outstanding contribution to modern organometallic chemistry. The authors thank the Ministerio de Economía y Competitividad (MINECO-FEDER CTQ2016-75816-C2-1-P and CTQ2015-70371-REDT) and Gobierno de Aragón-Fondo Social Europeo (E07_17R) for financial support. A.L. thanks the Gobierno de Aragón for a predoctoral fellowship.

■ REFERENCES

(1) Fernández-Moreira, V.; Gimeno, M. C. Heterobimetallic Complexes for Theranostic Applications. *Chem. - Eur. J.* **2018**, *24*, 3345−3353.

(2) Raza, M. K.; Gautam, S.; Garai, A.; Mitra, K.; Kondaiah, P.; Chakravarty, A. R. Monofunctional BODIPY-Appended Imidazoplatin for Cellular Imaging and Mitochondria-Targeted Photocytotoxicity. *Inorg. Chem.* **2017**, *56*, 11019−11029.

(3) Wenzel, M.; de Almeida, A.; Bigaeva, E.; Kavanagh, P.; Picquet, M.; Le Gendre, P.; Bodio, E.; Casini, A. New Luminescent Polynuclear Metal Complexes with Anticancer Properties: Toward Structure−Activity Relationships. *Inorg. Chem.* **2016**, *55*, 2544−2557.

(4) Tasan, S.; Zava, O.; Bertrand, B.; Bernhard, C.; Goze, C.; Picquet, M.; Le Gendre, P.; Harvey, P.; Denat, F.; Casini, A.; Bodio, E. BODIPY−Phosphane as a Versatile Tool for Easy Access to New Metal-Based Theranostics. *Dalton Trans.* **2013**, *42*, 6102−6109.

(5) (a) Lo, K.K.-W.; Zhang, K. Y.; Li, S. P.-Y. Recent Exploitation of Luminescent Rhenium(I) Tricarbonyl Polypyridine Complexes as Biomolecular and Cellular Probes. *Eur. J. Inorg. Chem.* **2011**, 3551−3568. (b) Lo, K. K.-W. Luminescent Rhenium(I) and Iridium(III) Polypyridine Complexes as Biological Probes, Imaging Reagents, and Photocytotoxic Agents. *Acc. Chem. Res.* **2015**, *48*, 2985−2995.
(6) (a) Thorp-Greenwood, F. L.; Platts, J. A.; Coogan, M. P. Experimental and Theoretical Characterisation of Phosphorescence from Rhenium Polypyridyl Tricarbonyl Complexes. *Polyhedron* **2014**, *67*, 505−512. (b) Kumar, A.; Sun, S.-S.; Lees, A. J. Photophysics and Photochemistry of Organometallic Rhenium Diimine Complexes. *Top. Organomet. Chem.* **2009**, *29*, 37−71. (c) Lees, A. J. Luminescence Properties of Organometallic Complexes. *Chem. Rev.* **1987**, *87*, 711−743.
(7) (a) Fernández-Moreira, V.; Marzo, I.; Gimeno, M. C. Luminescent Re(I) and Re(I)/Au(I) Complexes as Cooperative Partners in Cell Imaging and Cancer Therapy. *Chem. Sci.* **2014**, *5*, 4434−4446. (b) Luengo, A.; Fernández-Moreira, V.; Marzo, I.; Gimeno, M. C. Trackable Metallodrugs Combining Luminescent Re(I) and Bioactive Au(I) Fragments. *Inorg. Chem.* **2017**, *56*, 15159−15170.
(8) Simpson, V.; Casari, I.; Paternoster, S.; Skelton, B. W.; Falasca, M.; Massi, M. Defining the Anti-Cancer Activity of Tricarbonyl Rhenium Complexes: Induction of G2/M Cell Cycle Arrest and Blockade of Aurora-A Kinase Phosphorylation. *Chem. - Eur. J.* **2017**, *23*, 6518−6521.
(9) Siegmund, D.; Lorenz, N.; Gothe, Y.; Spies, C.; Geissler, B.; Prochnow, P.; Nuernberger, P.; Bandow, J. E.; Metzler-Nolte, N. Benzannulated Re(I)−NHC Complexes: Synthesis, Photophysical Properties and Antimicrobial Activity. *Dalton Trans.* **2017**, *46*, 15269−15279.
(10) (a) Jin, T.; He, D.; Li, W.; Stanton, C. J., III; Pantovich, S. A.; Majetich, G. F.; Schaefer, H. F., III; Agarwal, J.; Wang, D.; Li, G. CO2 Reduction with Re(I)−NHC Compounds: Driving Selective Catalysis with a Silicon Nanowire Photoelectrode. *Chem. Commun.* **2016**, *52*, 14258−14261. (b) Huckaba, J.; Sharpe, E. A.; Delcamp, J. H. Photocatalytic Reduction of CO2 with Re-Pyridyl-NHCs. *Inorg. Chem.* **2016**, *55*, 682−690. (c) Ng, C.-O.; Cheng, S.-C.; Chu, W.-K.; Tang, K.-M.; Yiu, S.-M.; Ko, C.-C. Luminescent Rhenium(I) Pyridyldiaminocarbene Complexes: Photophysics, Anion-Binding, and CO2-Capturing Properties. *Inorg. Chem.* **2016**, *55*, 7969−7979. (d) Wang, G.-F.; Liu, Y.-Z.; Chen, X.-T.; Zheng, Y.-X.; Xue, Z.-L. Synthesis, Structure and Luminescent Properties of Rhenium(I) Carbonyl Complexes Containing Pyrimidine-Functionalized *N*-Heterocyclic Carbenes. *Inorg. Chim. Acta* **2013**, *394*, 488−493.
(11) (a) Vaughan, J. G.; Reid, B. L.; Ramchandani, S.; Wright, P. J.; Muzzioli, S.; Skelton, B. W.; Raiteri, P.; Brown, D. H.; Stagni, S.; Massi, M. The Photochemistry of Rhenium(I) Tricarbonyl *N*-Heterocyclic Carbene Complexes. *Dalton Trans.* **2013**, *42*, 14100−14114. (b) Chan, C. Y.; Pellegrini, P. A.; Greguric, I.; Barnard, P. J. Rhenium and Technetium Tricarbonyl Complexes of *N*-Heterocyclic Carbene Ligands. *Inorg. Chem.* **2014**, *53*, 10862−10873. (c) Mukuta, T.; Simpson, P. V.; Vaughan, J. G.; Skelton, B. W.; Stagni, S.; Massi, M.; Koike, K.; Ishitani, O.; Onda, K. Photochemical Processes in a Rhenium(I) Tricarbonyl *N*-Heterocyclic Carbene Complex Studied by Time-Resolved Measurements. *Inorg. Chem.* **2017**, *56*, 3404−3413.
(12) (a) Raba, A.; Anneser, M. R.; Jantke, D.; Cokoja, M.; Hermann, W. A.; Kühn, F. E. Facile and Scalable Preparation of 2-Imidazolylpyridines. *Tetrahedron Lett.* **2013**, *54*, 3384−3387. (b) Zhuang, R.-T.; Lin, W.-J.; Zhuang, R. R.; Hwang, W.-S. Hg(II), Ag(I) and Au(I) Complexes With Aniline or Pyridine-Functionalized *N*-Heterocyclic Carbene. *Polyhedron* **2013**, *51*, 132−141.
(13) Casson, A.; Muzzioli, S.; Raiteri, P.; Skelton, B. W.; Stagni, S.; Massi, M.; Brown, D. H. *N*-Heterocyclic Carbenes as π*-Acceptors in Luminescent Re(I) Triscarbonyl Complexes. *Dalton Trans.* **2011**, *40*, 11960−11967.
(14) Stanton, C. J.; Machan, C. W.; Vandezande, J. E.; Jin, T.; Majetich, G. F.; Schaefer, H. F.; Kubiak, C. P.; Li, G.; Agarwal, J. Re(I) NHC Complexes for Electrocatalytic Conversion of CO2. *Inorg. Chem.* **2016**, *55*, 3136−3144.
(15) (a) Simpson, P. V.; Skelton, B. W.; Raiteri, P.; Massi, M. Photophysical and Photochemical Studies of Tricarbonyl Rhenium(I) *N*-Heterocyclic Carbene Complexes Containing Azide and Triazolate Ligands. *New J. Chem.* **2016**, *40*, 5797−5807. (b) Vaughan, J. G.; Reid, B. L.; Wright, P. J.; Ramchandani, S.; Skelton, B. W.; Raiteri, P.; Muzzioli, S.; Brown, D. H.; Stagni, S.; Massi, M. Photophysical and Photochemical Trends in Tricarbonyl Rhenium(I) *N*-Heterocyclic Carbene Complexes. *Inorg. Chem.* **2014**, *53*, 3629−3641.
(16) Li, X.-W.; Li, H.-Y.; Wang, G.-F.; Chen, F.; Li, Y.-Z.; Chen, X.-T.; Zheng, Y.-X.; Xue, Z.-L. Blue-Green Luminescent Rhenium(I) Tricarbonyl Complexes with Pyridine-Functionalized *N*-Heterocyclic Carbene Ligands. *Organometallics* **2012**, *31*, 3829−3835.
(17) Fernández-Moreira, V.; Sastre-Martín, H. Photophysical and Bioactivity Behavior of *Fac*-Rhenium(I) Derivatives Containing Ditopic Sulfurpyridine Ligands. *Inorg. Chim. Acta* **2017**, *460*, 127−133.
(18) Casula, A.; Nairi, V.; Fernández-Moreira, V.; Laguna, A.; Lippolis, V.; Garau, A.; Gimeno, M. C. Re(I) Derivatives Functionalised with Thioether Crowns Containing the 1,10-Phenanthroline Subunit as a New Class of Chemosensors. *Dalton Trans.* **2015**, *44*, 18506−18517.
(19) Sacksteder, L. A.; Zipp, A. P.; Brown, E. A.; Streich, J.; Demas, J. N.; DeGraff, B. Luminescence Studies of Pyridine.Alpha.-Diimine Rhenium(I) Tricarbonyl Complexes. *Inorg. Chem.* **1990**, *29*, 4335−4340.
(20) Cunniff, B.; Snider, G. W.; Fredette, N.; Hondal, R. J.; Heintz, N. H. A Direct and Continuous Assay for the Determination of Thioredoxin Reductase Activity in Cell Lysates. *Anal. Biochem.* **2013**, *443*, 34−40.
(21) (a) Fernández-Moreira, V.; Ortego, M. L.; Williams, C. F.; Coogan, M. P.; Villacampa, M. D.; Gimeno, M. C. Bioconjugated Rhenium(I) Complexes with Amino Acid Derivatives: Synthesis, Photophysical Properties, and Cell Imaging Studies. *Organometallics* **2012**, *31*, 5950−5957. (b) Wedding, J. L.; Harris, H. H.; Bader, C. A.; Plush, S. E.; Mak, R.; Massi, M.; Brooks, D. A.; Lai, B.; Vogt, S.; Werrett, M. V.; Simpson, P. V.; Skelton, B. W.; Stagni, S. Intracellular Distribution and Stability of a Luminescent Rhenium(I) Tricarbonyl Tetrazolato Complex Using Epifluorescence Microscopy in Conjunction with X-Ray Fluorescence Imaging. *Metallomics* **2017**, *9*, 382−390. (c) Balasingham, R. G.; Thorp-Greenwood, F. L.; Williams, C. F.; Coogan, M. P.; Pope, S. J. A. Biologically Compatible, Phosphorescent Dimetallic Rhenium Complexes Linked through Functionalized Alkyl Chains: Syntheses, Spectroscopic Properties, and Applications in Imaging Microscopy. *Inorg. Chem.* **2012**, *51*, 1419−1426.
(22) Sheldrick, G. M. "Crystal structure refinement with SHELXL". *Acta Crystallogr., Sect. C: Struct. Chem.* **2015**, *71*, 3−8.
(23) Ruiz-Leal, M.; George, S. An *In Vitro* Procedure for Evaluation of Early Stage Oxidative Stress in an Established Fish Cell Line Applied to Investigation of PHAH and Pesticide Toxicity. *Mar. Environ. Res.* **2004**, *58*, 631−635.
(24) Gibson, D.; Johnson, B. F. G.; Lewis, J. Metal β-Diketone Complexes. Part VI. Some B-Diketone Complexes of Copper(I), Silver(I), and Gold(I). *J. Chem. Soc. A* **1970**, *0*, 367−369.

DOI: 10.1021/acs.organomet.8b00601
Organometallics XXXX, XXX, XXX−XXX